




Article

Curcumin-Containing Orthopedic Implant Coatings Deposited on Poly-Ether-Ether-Ketone/Bioactive Glass/Hexagonal Boron Nitride Layers by Electrophoretic Deposition

Ranjot Singh Virk¹, Muhammad Atiq Ur Rehman^{1,2} , Muhammad Azeem Munawar³ , Dirk W. Schubert³, Wolfgang H. Goldmann⁴, Ján Dusza⁵ and Aldo R. Boccaccini^{1,*} 

¹ Institute of Biomaterials, Department of Materials Science and Engineering, University of Erlangen-Nuremberg, Cauerstr. 6, 91058 Erlangen, Germany

² Department of Materials Science and Engineering, Institute of Space Technology Islamabad, 1, Islamabad Highway, Islamabad 44000, Pakistan

³ Institute of Polymer Materials, University of Erlangen-Nuremberg, Martensstraße 7, 91058 Erlangen, Germany

⁴ Department of Biophysics, University of Erlangen-Nuremberg, Henkestr. 91, 91052 Erlangen, Germany

⁵ Institute of Material Research, Slovak Academy of Sciences, 040001 Kosice, Slovak Republic

* Correspondence: aldo.boccaccini@ww.uni-erlangen.de or aldo.boccaccini@fau.de

Received: 24 July 2019; Accepted: 28 August 2019; Published: 8 September 2019



Abstract: Electrophoretic deposition (EPD) was used to produce a multilayer coatings system based on chitosan/curcumin coatings on poly-ether-ether-ketone (PEEK)/bioactive glass (BG)/hexagonal boron nitride (h-BN) layers (previously deposited by EPD on 316L stainless steel) to yield bioactive and antibacterial coatings intended for orthopedic implants. Initially, PEEK/BG/h-BN coatings developed on 316L stainless steel (SS) substrates were analyzed for wear studies. Then, the EPD of chitosan/curcumin was optimized on 316L SS for suspension stability, thickness, and homogeneity of the coatings. Subsequently, the optimized EPD parameters were applied to produce chitosan/curcumin coatings on the PEEK/BG/h-BN layers. The multilayered coatings produced by EPD were characterized in terms of composition, microstructure, drug release kinetics, antibacterial activity, and in vitro bioactivity. Scanning electron microscopy (SEM) and Fourier transform infrared spectroscopy (FTIR) confirmed the deposition of chitosan/curcumin on the multilayer coating system. The release of curcumin upon immersion of multilayer coatings in phosphate-buffered saline (PBS) was confirmed by ultraviolet/visible (UV/VIS) spectroscopic analysis. The antibacterial effect of chitosan/curcumin as the top coating was determined by turbidity tests (optical density measurements). Moreover, the multilayer coating system formed an apatite-like layer upon immersion in simulated body fluid (SBF), which is similar in composition to the hydroxyapatite component of bone, confirming the possibility of achieving close bonding between bone and the coating surface.

Keywords: curcumin; chitosan; bioactive coatings; electrophoretic deposition; antibacterial coatings

1. Introduction

Worldwide, millions of patients use implanted medical devices, including hip/knee joints, pacemakers, cardiovascular stents, dental implants, and so on. Despite intensive research in the area of biomedical materials and notable progress in the field of implants and prosthetic devices, there is a further need to improve implant performance [1,2]. In the case of bone implants, for example, premature failure may occur because of adhesion of biofilms, following bacterial attachment on the biomaterial

surface [3,4], potentially leading to infection and loosening of implants [4–7]. Furthermore, metallic implants usually do not develop a strong bond with bone. For improvement of metal implant bioactivity, surface modification approaches are being put forward, which involve, for example, coating the implants with inorganic materials like bioactive glass, hydroxyapatite, and calcium-phosphate cements [6,7]. These bioceramic coatings facilitate biocompatibility, osteo-conductivity, osteo-inductivity, and may impart antimicrobial activity [8]. The technique of electrophoretic deposition (EPD) is a colloidal processing method that can be used conveniently to deposit coatings on conductive substrates, based on the principle of electric field-assisted deposition of charged particles or molecules present in stabilized suspensions [3,5,6,9,10]. Through a simple change in deposition parameters (voltage, time, and inter-electrode distance) the thickness and morphology of EPD layers can be managed. EPD is increasingly being considered as a technique of choice for the deposition of a vast range of bioactive materials and their composites on different substrates for biomedical applications [6]. For example, the EPDs of composite coatings of poly-ether-ether-ketone (PEEK) and bioactive glass (BG) were first reported by Boccaccini et al. [11], and recently the EPD kinetic mechanisms for PEEK-BG coatings have been studied by using Taguchi's experimental design [12]. PEEK is a thermoplastic polymer with an elastic modulus close to that of cortical bone, which enables PEEK to act as a suitable interface between the metallic implant and bone [13–15]. Bioactive glasses are an important group of bioactive inorganic materials, which can attach to bone tissue and have the ability to activate the body's own regenerative system by releasing biologically active ions [16–18]. Hexagonal boron nitride (h-BN) has been considered only in a few cases as a component of coatings for biomedical applications. h-BN has a structure similar to that of graphite. The layered structure of h-BN confers unique engineering properties to this material such as solid lubricant effects [19]. Moreover, h-BN has been investigated as dental cement and in cosmetic preparations. Investigations of coatings that contain h-BN for biomedical applications are relevant because h-BN may also prevent infections and can improve the wear behavior of PEEK composite coatings [20,21].

Chitosan is a natural polymer, which has various attractive properties such as a film-forming ability, drug carrier capability, non-toxicity, biodegradability, biocompatibility, and antibacterial effects [22–25]. Chitosan is a natural polysaccharide, which is used in several applications in the biomedical, environmental, agriculture, food and chemistry sectors, and in the textile industry. Chitosan can be utilized for the electrophoretic co-deposition of inorganic particles to develop composite coatings [24–27]. The mechanisms of EPD of chitosan and chitosan-particle composites have been extensively investigated [22,25,28]. Briefly, protonated chitosan molecules can adsorb on the surface of suspended particles and give a net positive charge around them, which allows particles to move toward the cathode during EPD. Moreover, positively charged chitosan molecules also migrate towards the cathode under an applied voltage [27,29].

Curcumin (1,7-bis(4-hydroxy-3-methoxyphenyl)-1,6-heptadiene-3,5-dione, diferuloylmethane) is a natural yellow herbal drug [30] and a spice derived from Zingiberaceae that has been used since ancient times in Ayurvedic medicine [31]. It has various pharmacological activities, including antioxidant, antimicrobial, and anti-inflammatory properties [32]. Research has shown that curcumin has the potential to treat diseases such as arthritis, pancreatitis, chronic anterior uveitis, and certain types of cancer [31,33] and it is also capable of decreasing inflammatory effects [6,31,33,34]. Since there are no previous studies discussing the mechanism of EPD of chitosan/curcumin coatings, we investigated in this study the EPD of chitosan/curcumin mixtures under different conditions. The chitosan/curcumin suspension exhibited a zeta potential of +35 mV at pH ~ 4.2. The positive value of zeta potential indicated that chitosan and curcumin will move towards the cathode upon the application of an external electric field. Moreover, it was observed that the addition of curcumin maintains the initial stability of the chitosan solution. Curcumin alone, upon dispersion in an ethanol–water solvent, showed a zeta potential value of +30 mV at pH ~ 4.2, indicating that both chitosan and curcumin would deposit at the cathode during EPD.

This research work, therefore, focuses on the production of new functional multilayer coatings based on chitosan/curcumin on PEEK/BG/h-BN layers by EPD. The top layer (chitosan/curcumin) serves as a degradable curcumin-releasing coating. In the bottom layer, the combination of PEEK and h-BN may lead to a coating with improved mechanical properties, while the addition of bioactive glass particles should enhance the bioactivity of the coatings, thus facilitating the bone-bonding ability and rendering the coatings of interest for orthopedic applications. Moreover, curcumin may be released in a sustained manner from the multilayer coating (chitosan/curcumin deposited on PEEK/BG/h-BN film) to provide antibacterial effects. The concept of multilayer coatings composed of PEEK and chitosan-based coatings obtained by EPD has been introduced recently [28]; however, the use of curcumin in the chitosan layer has been investigated for the first time in this study.

2. Experimental Procedure

2.1. Coating of Poly-Ether-Ether-Ketone/Bioactive Glass/Hexagonal Boron Nitride (PEEK/BG/h-BN)

BG powder (3.3 wt.%) of 4 μm diameter (D50) with nominal composition 45S5 BG (45 wt.% silicon oxide, 24.5 wt.% calcium oxide, 24.5 wt.% sodium oxide, and 6 wt.% phosphor pentoxide) and 6.6 wt.% monohydrate citric acid (VWR International, Darmstadt, Germany) were added in ethanol. The suspension was stirred magnetically for 3 min, and then ultrasonication was conducted for 2 h. Subsequently, 2 wt.% PEEK powder (704 XF, Victrex, Lancashire, UK) with 10 μm diameter (D50) and 0.5 wt.% h-BN powder (Henze BNP AG, Lauben, Germany) with 2 μm diameter (D50) was added into the suspension, which was stirred magnetically for 3 min followed by ultrasonication for 30 min. The details about the optimization of suspension composition have been reported previously [5]. Moreover, the addition of citric acid provided excessive anions in suspension, which led to the negative charges of PEEK, BG, and h-BN. 316L SS foils with dimensions of 1.5 cm width, 0.2 mm thickness, cut to a length of 3 cm, and cleaned with ethanol were used as the deposition substrate and counter electrodes for EPD. The spacing between electrodes, applied voltage, and deposition time were fixed at 1 cm, 90 V, and 90 s, respectively. Previous studies with detailed information on PEEK based coatings using EPD are available [5,12,14,35,36]. The PEEK/BG/h-BN coatings were heat-treated in a furnace (NaberthermTM GmbH, Lilienthal, Germany) at 375 °C for 30 min at a heating rate of 2 °C/min. The samples were cooled down slowly in the furnace (annealing) in order to avoid the formation of microcracks. The processing temperature was selected based on available information for heat treatment of PEEK [3,5,14,15,37].

2.2. Coatings of Chitosan/Curcumin

An amount of 0.5 g/L chitosan (medium average molecular weight with 75%–85% deacetylation degree) was dissolved in distilled water having 20 vol.% and acetic acid having 1 vol.% and stirred magnetically for 25 min. Ethanol with 79 vol.% was added to the chitosan-dissolved solution in order to reduce the possible hydrolysis of water during the EPD process, which may affect the homogeneity of the coatings, following previous studies [38,39]. Then, 1–5 g/L curcumin (Sigma AldrichTM, Darmstadt, Germany) was added to the prepared chitosan solution and stirred magnetically for 5 min. After several preliminary trials, it was elucidated that the optimum composition of curcumin in the suspension was 2.5 g/L to achieve a clear and stable solution for EPD. In this study, the composition range for curcumin was selected, based on the available literature, which confirmed that curcumin is antibacterial and cytocompatible within a selected range of compositions [32]. The suspension stability was determined by zeta-potential measurements, using a zetasizer (nano ZS equipment, Malvern InstrumentsTM, Malvern, UK). Initially, the EPD of chitosan/curcumin was optimized on stainless-steel substrates. Finally, the optimized parameters were applied on PEEK/BG/h-BN layers (previously coated by EPD on 316L SS), as described in Section 2.1. Table 1 shows the details of EPD parameters for chitosan/curcumin coatings.

Table 1. Electrophoretic deposition (EPD) parameters along with suspension-related processing characteristics of chitosan/curcumin coatings on the poly-ether-ether-ketone/bioactive glass/hexagonal boron nitride (PEEK/BG/h-BN) layer.

Suspension-Related Properties		Process Parameters of EPD	
Chitosan type	Medium molecular weight at 75%–85% deacetylation degree	Applied Voltage (V)	20
Chitosan conc. (g/L)	0.5	Time of deposition (min)	3
Curcumin conc. (g/L)	2.5	Distance between inter-electrode (mm)	10
Charging agent	Acetic acid (1 vol.%)	Substrate; counter electrode	PEEK/BG/h-BN; 316L SS
Zeta potential and pH	+37 mV and 4.3 pH	Coating thickness	70–80 μm (Multilayer coatings)
Suspension solvent	Ethanol (79 vol.), distilled water (20 vol.)	–	–

2.3. Characterization of Coatings

Scanning electron microscopy (SEM) (AURIGA CrossBeam; Carl Zeiss Microscopy GmbH, Oberkochen, Germany) was performed for investigation of the morphology of the fabricated coatings, and gold sputtering was used to prepare the samples for SEM. At 15 kV, energy dispersive X-ray (EDX) spectroscopy was used for compositional analysis of coatings (LEO 435VP, Carl Zeiss Microscopy GmbH). Fourier transform infrared (FTIR) spectroscopy (Shimadzu Corp, Kyoto, Japan) with attenuated total reflection (ATR) mode was conducted for functional group analysis. The thermal stability of coatings was analyzed using thermo-gravimetric analysis (TGA 2950, TA instruments, New Castle, DE, USA). Prior to the TGA measurements, coating layers were detached from the substrate. TGA was executed at a maximum temperature of 1000 °C under a dynamic air atmosphere at a heating rate of 10 °C/min. A laser profilometer (UBM™, ISC-2) was used for the measurement of surface roughness of fabricated coatings. Samples of dimensions (1.5 cm \times 1.5 cm) were used for each coating (three samples for each type was used), and an area of 1 mm \times 1 mm was specified for the measurements of surface roughness with a scanning velocity of 400 points per second. The average surface roughness (S_{av}) and maximum surface roughness (S_{max}) were determined using the LMT Surface View UBM™ software (1995).

Wear tests were conducted by using a tribometer (CSM instruments, Peseux, Switzerland) under a load of 7 N at room temperature using pin-on-disc dry sliding method, as reported in references [40,41]. The humidity (about 25%) was controlled by using a dehumidifier. Ceramic balls of alumina having 2 mm diameter were used as counter bodies. The disc containing PEEK/BG/h-BN coatings was rotated with a certain speed while a ceramic ball was inserted perpendicularly with respect to the disc surface. The sliding speed of 15 cm/s was maintained for covering a distance of 750 m. The coefficient of friction was measured during experimental runs. With a profilometer, the wear volume was calculated by utilizing the surface profile traces, which were recorded across the wear path perpendicular to the sliding direction.

A drug release test was conducted to check the curcumin release behavior from the multilayer composite coatings. The absorption peak was measured at 426 nm for the release of curcumin in multilayer coatings by using ultraviolet-visible spectroscopy (UV spectroscopy, specord 40, Jena, Germany) with WinASPECT software (version 2.5.8.0). The cumulative release of curcumin was studied for a total of 48 days. Coatings of specific dimensions (15 mm \times 15 mm) were dipped in 10 mL phosphate-buffered saline (PBS) solution, and the samples were placed in an incubator at 37 °C. Three samples were studied at each time point. During testing, 1 mL of buffered saline solution was

considered for the evaluation of drug release, meanwhile 1 mL fresh buffered saline solution was poured back to preserve physiological conditions. The percentage of cumulative drug release (ρ_x) was measured by using Equation (1) at each time point:

$$\rho_x = \left(\frac{m_x}{m_t} \right) \times 100 \quad (1)$$

where m_x is the mass of drug release at each individual time point, and m_t is the cumulative mass of the drug in multilayer coatings.

An antibacterial turbidity test was conducted for the multilayer composite coatings relative to the single-layer (PEEK/BG/h-BN) composite coatings, which were considered as reference. UV light for 45 min was used to sterilize samples. Ten milliliters of Lysogeny broth (LB) media were filled in plastic flasks, which were inoculated with Gram-positive (*Staphylococcus carnosus*) and Gram-negative (*Escherichia coli*) bacteria at an optical density of 0.015 (OD600nm). The samples were immersed in the prepared bacterial solution at 37 °C for 1, 2, 4, 24, 48, 96 and 168 h. At each time point, 1 mL of the solution was taken out and replaced with the fresh LB media. The optical density at 600 nm was measured for the extracts taken out at each time point.

To confirm the bioactivity of the multilayer coatings in terms of hydroxyapatite (HAp) formation as function of time, simulated body fluid (SBF) studies, as suggested by Kokubo et al. [42], were carried out. Multilayer samples (15 mm × 15 mm × 0.2 mm) were dipped into 50 mL of SBF, then incubated for 7 and 14 days in an orbital shaker at 90 RPM and 37 °C, refreshing the SBF every third day as postulated in literature [42]. For every time point samples were taken out from SBF, washed with distilled water and left to dry at ambient conditions. The possible creation of a hydroxyapatite layer on the coating surfaces was examined by FTIR and SEM/EDX.

3. Results and Discussion

3.1. Composite Coating of PEEK/BG/h-BN on 316L Stainless Steel (SS) (Single Layer)

SEM micrographs of composite coatings PEEK/BG/h-BN at different magnifications are shown in Figure 1A,C. Figure 1A shows that sintered PEEK/BG/h-BN coatings were homogenous and comparably rough. SEM images of the cross-section indicate that the PEEK/BG/h-BN layer had a fairly uniform thickness (Figure 1B,C). Coatings showing thickness in the range 70–80 μm were densely packed following the sintering process. Moreover, the coating thickness noticed in this study was in agreement with the literature [29]. Figure 1D confirms the presence of PEEK (C peak) and BG (Si, Ca, Na and P peaks) in the produced coatings. Previous studies have optimized the composition and characteristics of this type of coating [36].

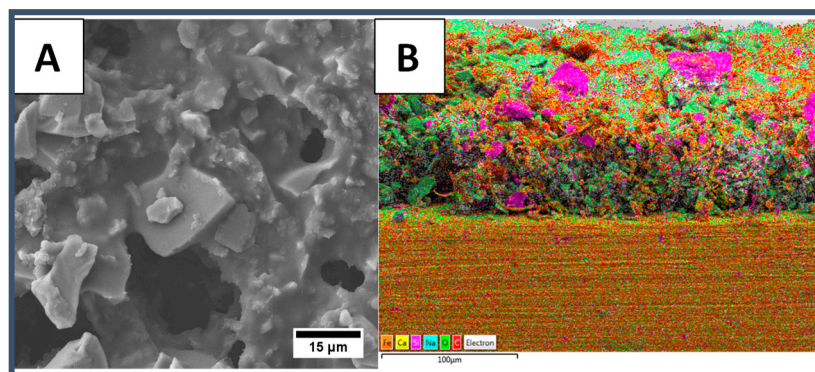


Figure 1. Cont.

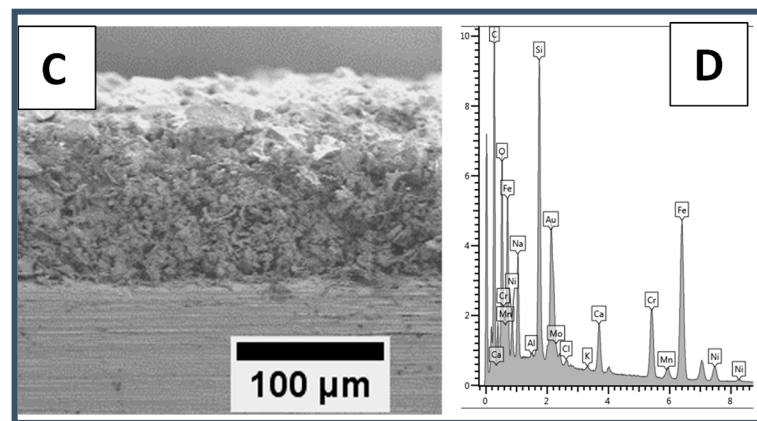


Figure 1. PEEK/BG/h-BN coatings produced by EPD at a voltage of 90 V for 90 s and sintered at 375 °C; (A) SEM image of the top surface, (B) EDX mapping at the cross-section, (C) SEM image at a cross-section, and (D) EDX analysis.

In our previous studies [5], PEEK/BG/h-BN coatings showed a convenient wetting behavior and good adhesion strength to stainless steel substrates. Moreover, the produced coatings were bioactive according to SBF studies [5]. The wear behavior of the coatings was investigated in the present study, given the relevance of this property for applications in orthopedic implants [12]. Wear refers to the deformation of materials during the mechanical process of relative motion between two or more contacting surfaces, which causes the surface to degrade. The surface of the implanted device can wear out, and this can primarily affect joint prosthesis [43]. Therefore, h-BN can be conveniently used, exploiting its layered (lubricating) structure, in combination with polymeric biomaterials to impart self-lubrication properties and wear resistance to the coatings.

In Figure 2, the results of wear tests under dry sliding conditions at a load of 7 N against alumina balls on PEEK, PEEK/BG, and PEEK/BG/h-BN coatings are presented. Throughout the whole span of the test, the friction behavior of all materials was stable. Afterward, the coefficient of friction (COF) remained stable for PEEK/BG and PEEK/BG/h-BN coatings. Few oscillations in the coefficient of friction of PEEK coatings were observed, which could be due to the nonuniform wear track in PEEK [44,45], as shown in confocal microscope images (Figure 3). The oscillations in the wear test of PEEK coatings were repeated with each revolution of the disc. Moreover, with an increase in the number of cycles, the amplitude of oscillations changed (Figure 3). However, COF remained stable over the sliding distance of 750 m. The results, thus, indicate that PEEK/BG/h-BN coatings sintered at 375 °C exhibited a constant and relatively low friction coefficient value (COF = 0.35) in comparison to the PEEK (COF = 0.26) and PEEK/BG (COF = 0.37) coatings. Moreover, PEEK/BG and PEEK/BG/h-BN coatings maintained the coefficient value over the sliding distance of 750 m, which illustrates the high wear resistance of the produced coatings. Values for the coefficient of friction of PEEK/BG and PEEK have been reported [15,45]. The reduction in COF of PEEK/BG/h-BN coatings in comparison to PEEK/BG coatings indicates the lubrication effect provided by the addition of h-BN, as expected [5].

Figure 3 shows a deep wear track for the PEEK, PEEK/BG, and PEEK/BG/h-BN coatings. However, the incorporation of h-BN in the coating decreased the COF, and no sign of wear was observed on the coatings after the wear test, which confirms the anticipated beneficial effect of adding h-BN to the base coating. The difference in the z-axis range in all samples was due to the difference in the average roughness of the three samples tested for each coating type. Therefore, it can be stated (on the basis of Figure 3) that no visible sign of wear was observed (in Figure 3C) for PEEK/BG/h-BN. However, Figure 3A clearly shows the wear pattern, as indicated by the red arrow. Moreover, it is suggested that SEM analyses of the samples after the wear test should be carried out to gain a clearer understanding of the wear behavior of the coatings and to ascertain the mechanisms of material removal from the different coatings.

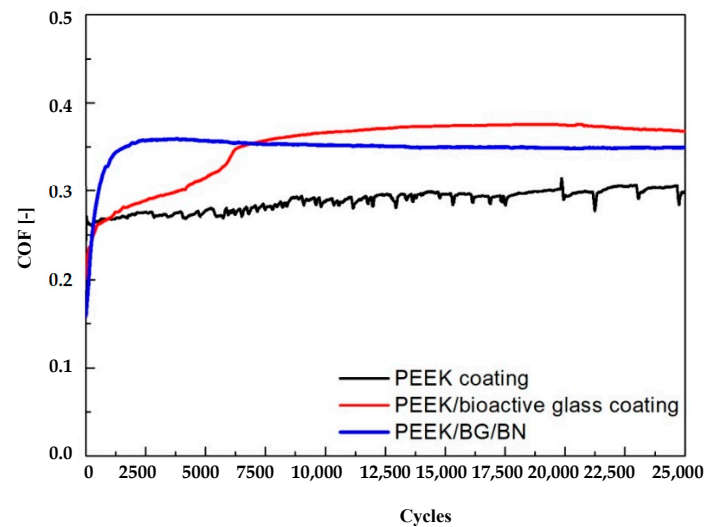


Figure 2. Time development of the coefficient of friction (COF) measured against an alumina ball at an applied load of 7 N for PEEK, PEEK/BG, and PEEK/BG/h-BN coatings.

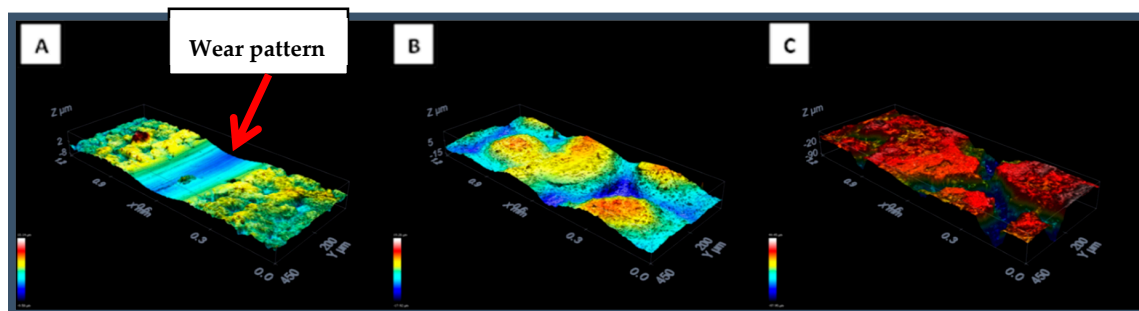


Figure 3. Confocal microscope images showing the wear track after the wear tests of (A) PEEK, (B) PEEK/BG, and (C) PEEK/BG/h-BN coatings.

3.2. Coating of Chitosan/Curcumin on 316L SS

The “hit and trial” method was used to optimize the EPD process for chitosan/curcumin coatings on 316L SS substrates. EPD of chitosan-based coatings was optimized in our previous studies [28,46], which illustrated that the optimum electrode distance was 1 cm (therefore, the distance between electrodes was kept at 1 cm in this study). Moreover, the deposition time was also studied in this work (data not shown here), which elucidated that the increase in deposition time led to inhomogeneities in the deposited coatings. Moreover, increasing the deposition time beyond three minutes caused sedimentation of the suspension (chitosan/curcumin), which resulted in poor-quality coatings. The effect of deposition voltage and time on the homogeneity of the produced coatings is illustrated in Figure 4. The figure shows that the chitosan/curcumin coatings obtained at 30 V and 3 min resulted in thick layers (Figure 4A), but the coatings were not homogenous. The coatings obtained at 15 V and 3 min showed poor adhesion to the substrate (Figure 4B). Moreover, the coatings obtained at 20 V and 3 min were fairly homogenous and showed an adhesion strength class of 4 B (Figure 4C). Therefore, for the EPD process, we set the values of 20 V, 3 min, and 1 cm for the applied voltage, deposition time, and spacing between electrodes, respectively. By using the mentioned EPD parameters, fairly homogenous coatings were obtained, as shown by the microscopic images in Figure 4 and at higher magnification SEM images in Figure 5.

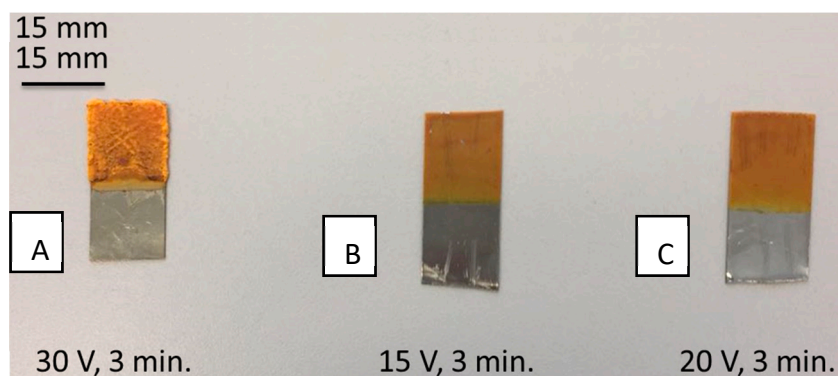


Figure 4. Digital camera images for the chitosan/curcumin composite coatings on 316L stainless steel (SS) produced at: (A) 30 V and 30 minutes, (B) 15V and 3 minutes, and (C) 20 V and 3 minutes by keeping the inter-electrode distance at 10 mm.

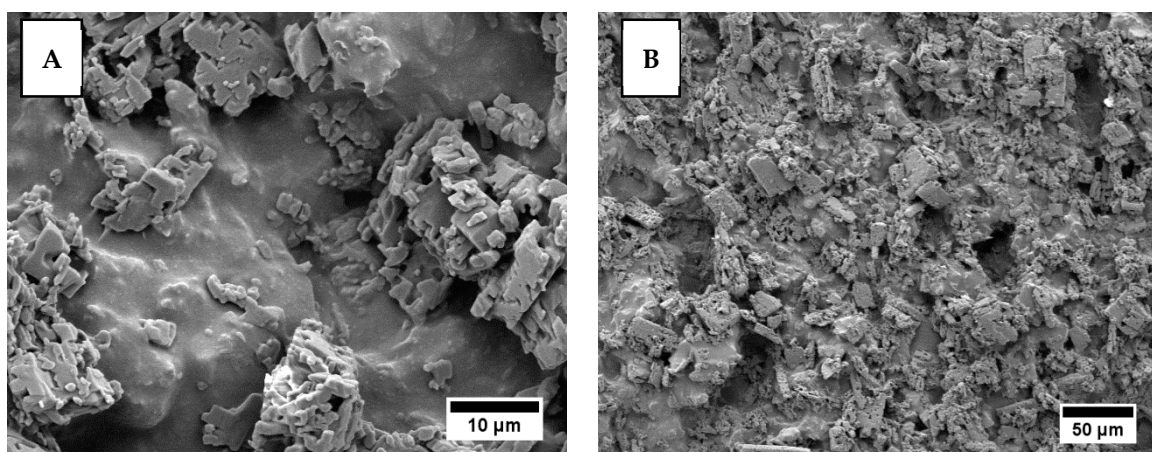


Figure 5. SEM images at two magnifications of chitosan/curcumin coatings produced by EPD on 316L SS at 20 V and 3 min: (A) 500× and (B) 5000×.

The curcumin particles were dispersed homogeneously in the chitosan matrix. However, the produced coatings were rough and porous, as shown in Figure 5. SEM images at two magnifications of chitosan/curcumin coatings produced by EPD on 316L SS at 20 V and 3 min: (A) 500× and (B) 5000×—are shown.

FTIR spectroscopy results showed the functional group analyses of chitosan, curcumin, and chitosan/curcumin coatings. As observed in Figure 6, FTIR spectra of curcumin indicate the presence of C–H bands at 714, 777, and 806 cm^{-1} , respectively. The peaks at 1603 cm^{-1} and 1624 cm^{-1} indicate the presence of carbonyl groups in curcumin. Moreover, the peak at 1510 cm^{-1} indicates the presence of ethylene group in curcumin [33]. The stretching bands and peaks of C–H at 714, 786, and 806 cm^{-1} , –C–O– bands at 1603 and 1624 cm^{-1} , and the ethylene group at 1510 cm^{-1} confirmed the presence of curcumin and chitosan in our fabricated chitosan/curcumin composite coatings. However, there is a slight shift in the chitosan-related peaks to the lower wavenumbers in the FTIR spectra of chitosan/curcumin coatings. For example, the C–O band at 1054 cm^{-1} [47,48] shifted to 1025 cm^{-1} , the C–H band at 1401 cm^{-1} shifted to 1375 cm^{-1} , and the N–H band at 1530 cm^{-1} shifted to 1506 cm^{-1} [49,50]. The slight shift in the chitosan-related peaks in the FTIR spectra of chitosan/curcumin coatings indicated the possibility of bonding between chitosan and curcumin.

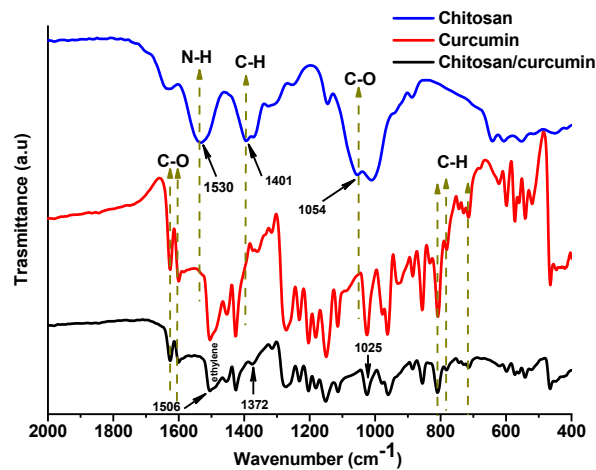


Figure 6. FTIR spectra of curcumin and chitosan coatings on 316L SS and chitosan/curcumin composite coatings on 316L SS. The relevant peaks are discussed in the text.

3.3. Coatings of Chitosan/Curcumin on PEEK/BG/h-BN Layers (Multilayer Coatings)

3.3.1. SEM Microstructure Analyses

An SEM picture of the coating surface shows the successful deposition of chitosan/curcumin on PEEK/BG/h-BN layer (Figure 7A,B). The chitosan/curcumin coating covered the PEEK/BG/h-BN layer by filling in the pores completely (in most of the instances). However, it can be observed that the chitosan matrix embedded with curcumin formed a film on the PEEK/BG/h-BN layer, as shown in Figure 7A,B. Figure 7C shows the SEM image at the cross-section of the multilayer coating. The thickness of the multilayer coatings was estimated to be 60–70 μm (Figure 7C,D). Moreover, the EDX line analysis on the cross-section further confirmed that the intensity of C, Si, Ca and Na increased strongly, from 70 to 140 μm , along the cross-section of the multilayer coating (Figure 7D).

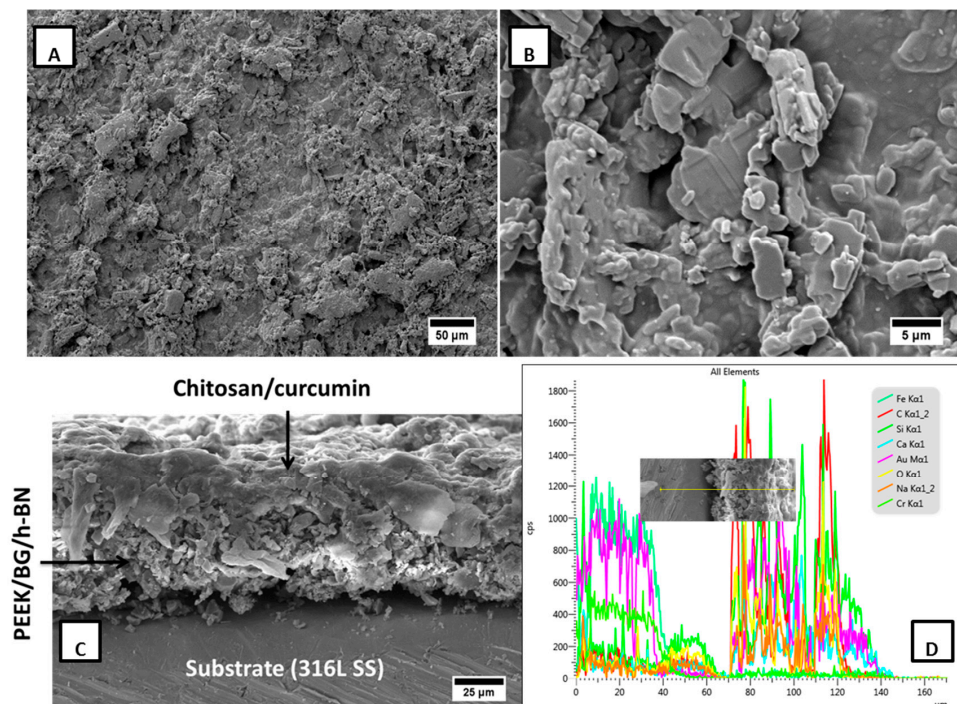


Figure 7. SEM micrographs for EPD of chitosan/curcumin composite coatings produced on PEEK/BG/h-BN layers at 20 V for 3 min at: (A) 500 \times , (B) 5000 \times , (C) cross-section, (D) compositional cross-section.

3.3.2. FTIR Analysis

The spectra of chitosan/curcumin and the PEEK/BG/h-BN layer are shown in Figure 8. The characteristic peaks of chitosan were found in the multilayer as well as in chitosan/curcumin single coatings; the carbonyl functional group (C=O) of chitosan was found at 1080 cm^{-1} [47,48,51]. The broad band at about 1022 cm^{-1} may have appeared because of the overlap of the C=O bond in chitosan and the bond corresponding to network modifiers in the glass structure [25,49,51]. Furthermore, the peak found at 1408 cm^{-1} is assigned to the asymmetrical bending in C-H, and the peak at about 1570 cm^{-1} is attributed to N-H bonding vibration of chitosan [52,53]. The relevant bands for curcumin in multilayer coatings were: C-H band at $714, 806$ and 786 cm^{-1} , -C-O- band at 1603 and 1624 cm^{-1} , and the ethylene group at 1510 cm^{-1} [33].

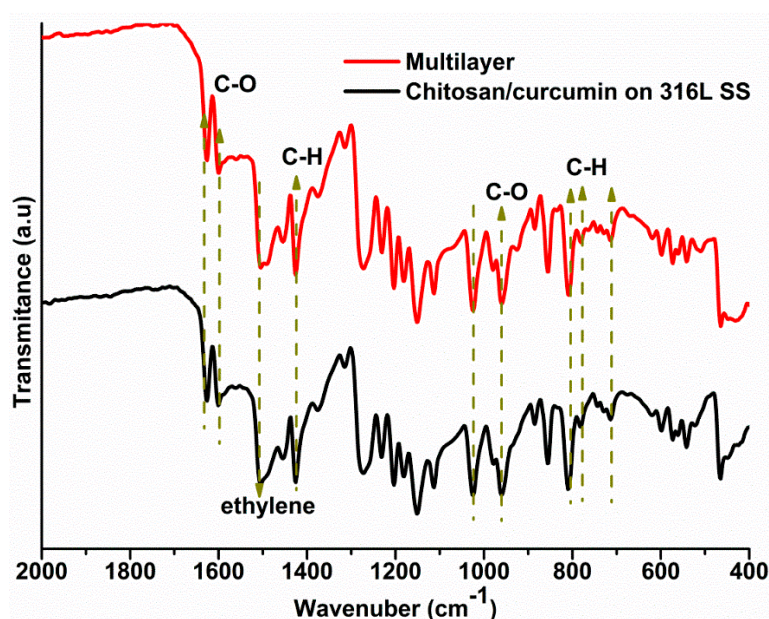


Figure 8. FTIR spectra of chitosan/curcumin coatings on SS and on PEEK/BG/h-BN layers (multilayer) produced by EPD.

3.3.3. Thermogravimetric Analysis (TGA)

Thermal degradation patterns of the PEEK/BG/h-BN (single layer) and chitosan/curcumin coatings on PEEK/BG/h-BN layers (multilayer) are shown in Figure 9. The thermogram of the single layer shows a mass loss (about 0.5%) from ambient to $100\text{ }^{\circ}\text{C}$, which can be ascribed to the removal of dampness and further losses up to $200\text{ }^{\circ}\text{C}$ for complete dehydration of bound water (about 1.5%). The region between 100 to $200\text{ }^{\circ}\text{C}$ shows a typical transition state of PEEK at $150\text{ }^{\circ}\text{C}$, considered the glass transition temperature (T_g) of PEEK. The region between 340 to $440\text{ }^{\circ}\text{C}$ indicates the melting and flow behavior of PEEK without significant mass loss. The onset of degradation of PEEK started at $440\text{ }^{\circ}\text{C}$ [28], and all polymeric chains underwent scission into tiny parts at about $472\text{ }^{\circ}\text{C}$, with complete burning at about $550\text{ }^{\circ}\text{C}$, having approximately a 79% residue corresponding to the inorganic components of BG and h-BN.

The thermogram of the multilayer coating shows a different trend with steeper and earlier degradation behaviors relative to the single-layer coating. Between ambient temperature to the $200\text{ }^{\circ}\text{C}$ region, the removal of bound water as well as melting and scissoring of chitosan and curcumin are responsible for the mass loss. From 200 to $380\text{ }^{\circ}\text{C}$, the multilayer coating showed continuous, significant mass loss (ca. 6%) by burning off chitosan and curcumin. As compared to the single-layer coating, the onset of degradation of PEEK in the multilayer coating starts earlier (at approximately $400\text{ }^{\circ}\text{C}$). Finally, the decomposition temperatures of both single-layer and multilayer coatings were very similar at approximately $550\text{ }^{\circ}\text{C}$.

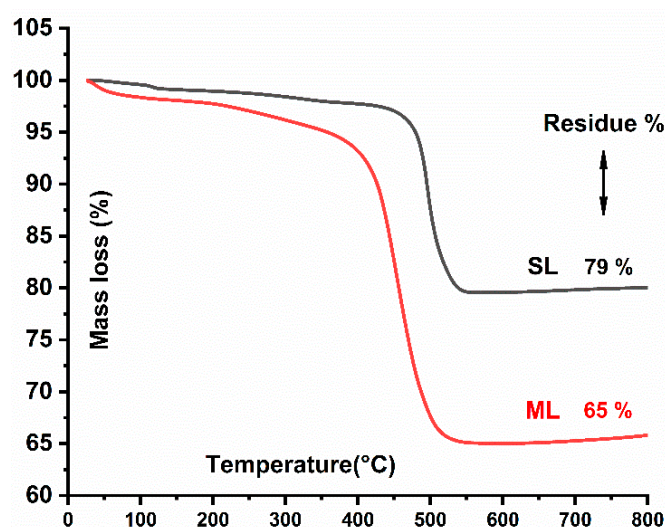


Figure 9. Thermogravimetric analysis of single-layer (SL) and multilayer (ML) coatings.

3.3.4. Roughness Measurements

Cell attachment and proliferation are important parameters, which are affected by roughness of the coating surfaces. PEEK/BG/h-BN composite coatings showed a mean roughness (R_a) of $1.8 \pm 0.1 \mu\text{m}$ and a maximum roughness (R_z) of $9 \pm 1 \mu\text{m}$ (Table 2). However, the multilayer coatings showed a decrease in the roughness values ($R_a = 1.5 \mu\text{m}$) in comparison to that of the PEEK/BG/h-BN layer ($R_a = 1.8 \mu\text{m}$), which confirmed that the chitosan/curcumin layer filled the pores and decreased the roughness of the multilayer layer coatings compared to that of the PEEK/BG/h-BN layer. Moreover, the filling of pores present in PEEK/BG/h-BN layer with chitosan/curcumin could also be a useful feature to control the release of the drug for longer periods of time. This phenomenon has been suggested previously in similar PEEK/chitosan-based multilayer coatings [28]. The roughness results obtained in this study are in agreement with the previous results reported by Rehman et al. [28].

Table 2. Roughness measurements for PEEK/BG/h-BN coatings sintered at $375 \text{ }^\circ\text{C}$ and for chitosan/curcumin coating on the PEEK/BG/h-BN layer.

Substrate	Mean Roughness (R_a) μm	Maximum Roughness (R_z) μm
Chitosan/Curcumin on the PEEK/BG/h-BN layer (multilayer)	1.5 ± 0.2	9 ± 1
PEEK/BG/h-BN sintered at $375 \text{ }^\circ\text{C}$	1.8 ± 0.1	9 ± 1

3.3.5. Drug Release Study

Sustained drug release systems for local drug delivery is important to investigate the effectiveness of the drug against bacterial infection and in reducing the danger of cytotoxicity [28], which can accelerate the curing process at the defected site [54,55].

The drug release curve can be studied in three main regions (Figure 10). Region I indicates the initial release (27% of the drug) during the first three days, which was mainly attributed to the diffusion of the molecules from the surface and smaller pores in the coatings [4,56]. The immersion of the multistructured coatings in phosphate-buffered saline (PBS) led to degradation of the chitosan (matrix), which caused a relative burst in the drug release rate. Therefore, it can be concluded that during the first day, curcumin was mainly released according to a diffusion mechanism [4,57]. However, after one day, the combination of degradation and diffusion triggered the drug release kinetics, and almost 47% of the drug was released during the first 10 days of immersion in PBS (region II) [58].

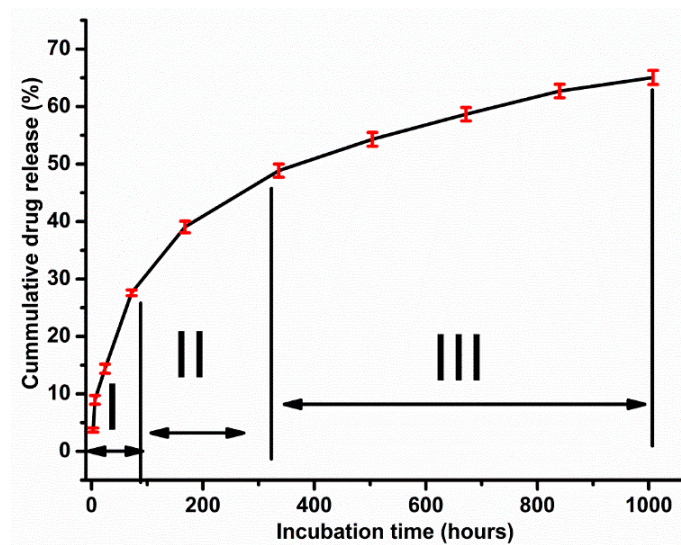


Figure 10. Cumulative release of curcumin in phosphate-buffered saline (PBS) from EPD coatings of chitosan/curcumin deposited on PEEK/BG/h-BN layers, showing 3 release stages: I, II and III. (The error bars indicate (\pm) standard deviation for three individual experiments, and each experiment contains 10 samples, $n = 30$).

In region III, about 65% of the drug was released. The drug release was relatively slow, which could be due to the fact that the chitosan matrix degraded completely, but some amount of the drug may have remained in deeper pores of the underlying PEEK/BG/h-BN layer. Thus, the higher roughness of the PEEK/BG/h-BN layer facilitates the sustained release of curcumin over a long period of time, as shown in Figure 10.

3.3.6. Antibacterial Studies

The antibacterial activities of multilayer and single-layer coatings were determined by turbidity tests (optical density measurements). The antibacterial activity of chitosan/curcumin coatings on PEEK/BG/h-BN layer was investigated for *S. carnosus* (Gram-positive) and *E. coli* (Gram-negative). Figure 11A shows that chitosan/curcumin coating on PEEK/BG/h-BN layers strongly decreased the optical density of the *S. carnosus* solution compared to the reference sample (i.e., PEEK/BG/h-BN). It was inferred that the multilayer coatings inhibited the growth of the Gram-positive bacteria.

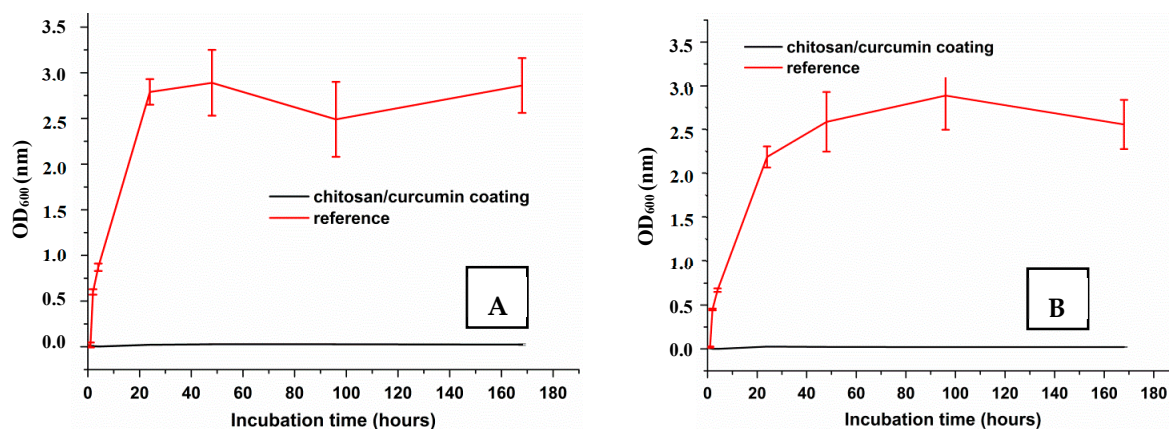


Figure 11. Antibacterial susceptibility test, showing the effect of chitosan/curcumin coatings on PEEK/BG/h-BN layers for Gram-positive (A) and Gram-negative (B) bacteria over the incubation period of 1 week (The error bars indicate (\pm) standard deviation for three individual experiments, and each experiment contain 10 samples, $n = 30$).

Figure 11B shows the effect of the chitosan/curcumin coating on *E. coli*. It was observed that the optical density of the *E. coli* solution, including reference samples, was much higher than that of the multilayer coatings, which indicated the antibacterial effect the chitosan/curcumin layer. It was concluded that the curcumin-loaded coatings possessed antibacterial effects against Gram-positive and Gram-negative bacteria, thus confirming the suitability of chitosan/curcumin coatings on PEEK/BG/h-BN layers for antiseptic orthopedic implants.

The exact antibacterial mechanism of curcumin has not yet been clearly elucidated. It has been reported in the literature that the biological activity associated with curcumin primarily is due to its antioxidant behavior [32]. Curcumin is considered as amphipathic and lipophilic molecule; curcumin can enter into liposome bilayers, which increases their permeability. It has been reported that curcumin alters the properties of bacteria membranes, leading, for example, to the thinning and disruption of the membrane. Thus, it is hypothesized that the antibacterial behavior of curcumin is related to perturbation of the bacterial cell wall and membrane by the amphipathic and lipophilic molecules of curcumin. Thus, curcumin can enter into the bacteria (Gram-positive and Gram-negative) body, disrupting the activity of DNA and causing bacterial cell death [32]. A similar behavior of curcumin against *S. aureus* has been reported in the literature [59]. Moreover, it was suggested that curcumin may be combined with other antibacterial agents/molecules to exhibit a stronger antibacterial effect.

3.3.7. Simulated Body Fluid (SBF) Studies

The variations in the morphology of the coating surfaces during immersion in SBF were observed by SEM (Figure 12), particularly assessing the formation of pores and the growth of a nanostructured apatite layer. The crystal size of the apatite-like structures increased with increasing time of immersion in SBF. Within the three days of immersion in SBF, plate-like hydroxyapatite structures were produced on the surface of coatings [25,38]. Since the iso-electric point (IEP) of multilayer coatings was lower than the value of 7.4 pH, the multilayer coatings were negatively charged in SBF and attracted calcium ions, leading to the growth of plate-like apatite enriched with calcium [28].

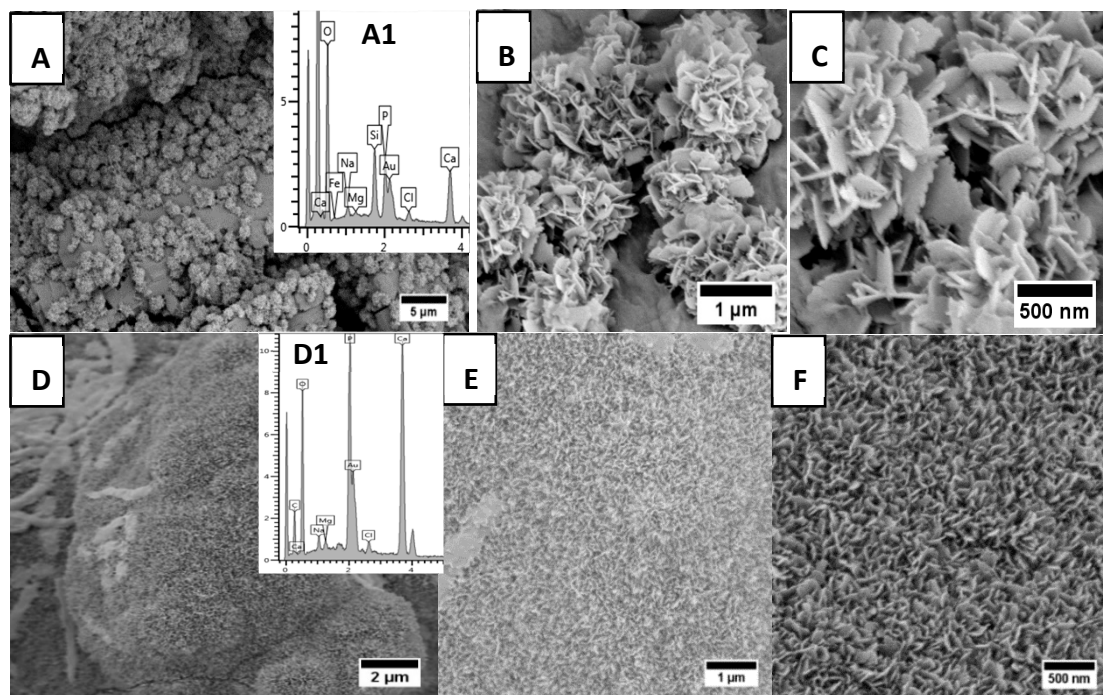


Figure 12. SEM images of the surface of the multilayer coating after treatment in SBF at different magnifications after 7 days [(A–C), corresponding EDX spectra (A1)] and after 14 days [(D–F) and corresponding EDX spectra (D1)].

The growth of apatite on the surface of the multilayer coatings was also proved by EDX results, which are shown in the inset graphs of Figure 12A,D. An increase in the intensity of phosphorus and calcium peaks, and the reduction in the intensity of silicon peaks, indicate the development of a calcium phosphate layer on the surface of multilayer coatings [60].

Moreover, the FTIR study showed the development of new bonds during immersion of multilayer coatings in SBF, as demonstrated in Figure 13. The spectra revealed a reduction in the intensity of the peaks related to BG (Si–O–Si at 459 cm^{-1} [25]) and amide-I peaks of chitosan after 3 days. Moreover, amide-II peaks (1558 and 1406 cm^{-1} [38]) disappeared after 3 days of immersion, which indicates degradation of chitosan. The fresh phosphate peaks (564 , 605 , 963 and 1030 cm^{-1} [25,61]) and carbonate peaks (868 and 1418 cm^{-1} [25,38]) suggest the formation of carbonated hydroxyapatite. The corresponding decrease in the intensity of the peaks related to BG (461 , 650 and 902 cm^{-1} [61]) after 1 days of immersion in SBF confirms the onset of dissolution of BG particles through the release of calcium and phosphate ions [16,61]. Actually, the formation of carbonated HA is the aim of adding BG to the base coatings, as such an HA surface layer will boost the bone bonding capability of the coatings [16,62].

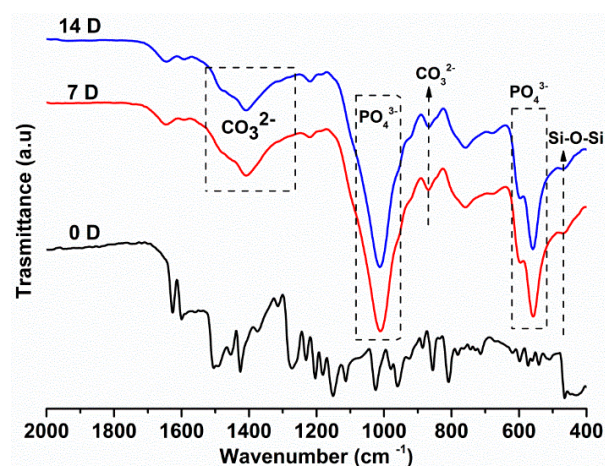


Figure 13. FTIR spectra of multilayer coatings before and after treatment in SBF for 7 and 14 days. The peaks of relevance are discussed in the text.

4. Conclusions

PEEK/BG/h-BN composite coatings deposited on 316L stainless steel provided an adequate substrate for the deposition of chitosan/curcumin composite coatings by EPD. The successful deposition of chitosan/curcumin on PEEK/BG/h-BN layers was confirmed by SEM and FTIR results. Moreover, the presence of curcumin was confirmed by UV/VIS and FTIR analyses. Chitosan/curcumin coatings fill up the pores in the PEEK/BG/h-BN layer to some extent, thus reducing the overall roughness of the multilayer coatings. Chitosan/curcumin coatings did not affect the initial in vitro bioactivity of the PEEK/BG/h-BN layer but promoted the formation of an apatite-like layer when immersed in SBF. Multilayer coatings showed a sustained release of curcumin, and the curcumin-loaded coatings were shown to possess strong antibacterial effects against Gram-positive and Gram-negative bacteria, confirming their suitability for orthopedic implants. Forthcoming work will focus on cell culture studies on the new curcumin-containing coatings. Moreover, the same coating approach by EPD should be investigated on different biomaterials, for example, by replacing 316 SS with titanium.

Author Contributions: Conceptualization, R.S.V. and A.R.B.; methodology, R.S.V., M.A.M., J.D. and M.A.U.R.; validation, R.S.V., M.A.M. and D.W.S.; formal analysis, R.S.V., M.A.U.R., J.D. and A.R.B.; investigation, R.S.V.; resources, R.S.V., D.W.S., J.D. and A.R.B.; writing—original draft preparation, R.S.V.; writing—review and editing, R.S.V., M.A.U.R., M.A.M., D.W.S., W.H.G. and A.R.B.; visualization, R.S.V., W.H.G., J.D. and M.A.U.R.; supervision, A.R.B. and W.H.G.; project administration, A.R.B.

Funding: This research received no external funding.

Acknowledgments: The authors would like to thank Alina Grünwald and Qaisar Nawaz for their support in the experimental work at the Institute of Biomaterials, Department of Material Science and Engineering, University of Erlangen-Nuremberg.

Conflicts of Interest: The authors have no conflict of interest to declare.

References

1. Doloff, J.C.; Veisoh, O.; Vegas, A.J.; Tam, H.H.; Farah, S.; Ma, M.; Li, J.; Bader, A.; Chiu, A.; Sadraei, A.; et al. Colony stimulating factor-1 receptor is a central component of the foreign body response to biomaterial implants in rodents and non-human primates. *Nat. Mater.* **2017**, *16*, 671–680. [[CrossRef](#)] [[PubMed](#)]
2. Montgomery, M.; Ahadian, S.; Huyer, L.D.; Rito, M.L.; Civitarese, R.A.; Vanderlaan, R.D.; Wu, J.; Reis, L.A.; Momen, A.; Akbari, S.; et al. Flexible shape-memory scaffold for minimally invasive delivery of functional tissues. *Nat. Mater.* **2017**, *16*, 1038. [[CrossRef](#)] [[PubMed](#)]
3. Baştan, F.E.; Rehman, M.A.U.; Avcu, Y.Y.; Avcu, E.; Üstel, F.; Boccaccini, A.R. Electrophoretic co-deposition of PEEK-hydroxyapatite composite coatings for biomedical applications. *Colloids Surf. B Biointerfaces* **2018**, *169*, 176–182. [[CrossRef](#)] [[PubMed](#)]
4. Simchi, A.; Tamjid, E.; Pishbin, F.; Boccaccini, A.R. Recent progress in inorganic and composite coatings with bactericidal capability for orthopaedic applications, Nanomedicine Nanotechnology. *Biol. Med.* **2011**, *7*, 22–39. [[CrossRef](#)]
5. Virk, R.S.; Rehman, M.A.U.; Boccaccini, A.R. PEEK based biocompatible coatings incorporating h-BN and bioactive glass by electrophoretic deposition. *ECS Trans.* **2018**, *82*, 89–95. [[CrossRef](#)]
6. Boccaccini, A.R.; Keim, S.; Ma, R.; Li, Y.; Zhitomirsky, I. Electrophoretic deposition of biomaterials. *J. R. Soc. Interface* **2010**, *7* (Suppl. S5), S581–S613. [[CrossRef](#)]
7. Zhang, B.G.X.; Myers, D.E.; Wallace, G.G.; Brandt, M.; Choong, P.F.M. Bioactive coatings for orthopaedic implants-recent trends in development of implant coatings. *Int. J. Mol. Sci.* **2014**, *15*, 11878–11921. [[CrossRef](#)]
8. Jones, J.R. Reprint of: Review of bioactive glass: From hench to hybrids. *Acta Biomater.* **2015**, *23*, S53–S82. [[CrossRef](#)]
9. Besra, L.; Liu, M. A review on fundamentals and applications of electrophoretic deposition (EPD). *Prog. Mater. Sci.* **2007**, *52*, 1–61. [[CrossRef](#)]
10. Ferrari, B.; Moreno, R. EPD kinetics: A review. *J. Eur. Ceram. Soc.* **2010**, *30*, 1069–1078. [[CrossRef](#)]
11. Boccaccini, A.R.; Peters, C.; Roether, J.A.; Eifler, D.; Misra, S.K.; Minay, E.J. Electrophoretic deposition of polyetheretherketone (PEEK) and PEEK/Bioglass[®] coatings on NiTi shape memory alloy wires. *J. Mater. Sci.* **2006**, *41*, 8152–8159. [[CrossRef](#)]
12. Rehman, M.A.U.; Bastan, F.E.; Haider, B.; Boccaccini, A.R. Electrophoretic deposition of PEEK/bioactive glass composite coatings for orthopedic implants: A design of experiments (DoE) study. *Mater. Des.* **2017**, *130*, 223–230. [[CrossRef](#)]
13. Kurtz, S.M.; Devine, J.N. PEEK biomaterials in trauma, orthopedic, and spinal implants. *Biomaterials* **2007**, *28*, 4845–4869. [[CrossRef](#)] [[PubMed](#)]
14. Moskalewicz, T.; Seuss, S.; Boccaccini, A.R. Microstructure and properties of composite polyetheretherketone/Bioglass[®] coatings deposited on Ti–6Al–7Nb alloy for medical applications. *Appl. Surf. Sci.* **2013**, *273*, 62–67. [[CrossRef](#)]
15. Sak, A.; Moskalewicz, T.; Zimowski, S.; Cieniek, Ł.; Dubiel, B.; Radziszewska, A.; Kot, M.; Łukaszczyk, A. Influence of polyetheretherketone coatings on the Ti–13Nb–13Zr titanium alloy’s bio-tribological properties and corrosion resistance. *Mater. Sci. Eng. C* **2016**, *63*, 52–61. [[CrossRef](#)] [[PubMed](#)]
16. Hench, L.L. Bioceramics. *J. Am. Ceram. Soc.* **1998**, *28*, 1705–1728. [[CrossRef](#)]
17. Hench, L.L. Bioceramics: From concept to clinic. *J. Am. Ceram. Soc.* **1991**, *74*, 1487–1510. [[CrossRef](#)]
18. Hench, L.L. The story of Bioglass[®]. *J. Mater. Sci. Mater. Med.* **2006**, *17*, 967–978. [[CrossRef](#)]
19. Lu, F.; Wang, F.; Cao, L.; Kong, C.Y.; Huang, X. Hexagonal boron nitride nanomaterials: Advances towards bioapplications. *Nanosci. Nanotechnol. Lett.* **2012**, *4*, 949–961. [[CrossRef](#)]
20. Raddaha, N.S.; Cordero-Arias, L.; Cabanas-Polo, S.; Virtanen, S.; Roether, J.A.; Boccaccini, A.R. Electrophoretic deposition of chitosan/h-BN and chitosan/h-BN/TiO₂ composite coatings on stainless steel (316L) substrates. *Materials* **2014**, *7*, 1814–1829. [[CrossRef](#)]

21. Tharajak, J.; Palathai, T.; Sombatsompop, N. Morphological and physical properties and friction/wear behavior of h-BN filled PEEK composite coatings. *Surf. Coat. Technol.* **2015**, *273*, 20–29. [[CrossRef](#)]
22. Zhitomirsky, D.; Roether, J.A.; Boccaccini, A.R.; Zhitomirsky, I. Electrophoretic deposition of bioactive glass/polymer composite coatings with and without HA nanoparticle inclusions for biomedical applications. *J. Mater. Process. Technol.* **2009**, *209*, 1853–1860. [[CrossRef](#)]
23. Pawlik, A.; Rehman, M.A.U.; Nawaz, Q.; Bastan, F.E.; Sulka, G.D.; Boccaccini, A.R. Fabrication and characterization of electrophoretically deposited chitosan-hydroxyapatite composite coatings on anodic titanium dioxide layers. *Electrochim. Acta* **2019**, *307*, 465–473. [[CrossRef](#)]
24. Radda'a, N.S.; Goldmann, W.H.; Detsch, R.; Roether, J.A.; Cordero-Arias, L.; Virtanen, S.; Moskalewicz, T.; Boccaccini, A.R. Electrophoretic deposition of tetracycline hydrochloride loaded halloysite nanotubes chitosan/bioactive glass composite coatings for orthopedic implants. *Surf. Coat. Technol.* **2017**, *327*, 146–157. [[CrossRef](#)]
25. Pishbin, F.; Mouriño, V.; Gilchrist, J.B.; McComb, D.W.; Kreppel, S.; Salih, V.; Ryan, M.P.; Boccaccini, A.R. Single-step electrochemical deposition of antimicrobial orthopaedic coatings based on a bioactive glass/chitosan/nano-silver composite system. *Acta Biomater.* **2013**, *9*, 7469–7479. [[CrossRef](#)] [[PubMed](#)]
26. Song, J.; Chen, Q.; Zhang, Y.; Diba, M.; Kolwijck, E.; Shao, J.; Jansen, J.A.; Yang, F.; Boccaccini, A.R.; Leeuwenburgh, S.C.G. Electrophoretic deposition of chitosan coatings modified with gelatin nanospheres to tune the release of antibiotics. *ACS Appl. Mater. Interfaces* **2016**, *8*, 13785–13792. [[CrossRef](#)]
27. Simchi, A.; Pishbin, F.; Boccaccini, A.R. Electrophoretic deposition of chitosan. *Mater. Lett.* **2009**, *63*, 2253–2256. [[CrossRef](#)]
28. Atiq, M.; Rehman, U.; Bastan, F.E.; Nawaz, Q.; Goldmann, W.H.; Maqbool, M.; Virtanen, S.; Boccaccini, A.R. Electrophoretic deposition of lawsone loaded bioactive glass (BG)/chitosan composite on polyetheretherketone (PEEK)/BG layers as antibacterial and bioactive coating. *J. Biomed. Mater. Res. Part A* **2018**, *12*, 3111–3122. [[CrossRef](#)]
29. Pishbin, F.; Simchi, A.; Ryan, M.P.; Boccaccini, A.R. Electrophoretic deposition of chitosan/45S5 bioglass composite coatings for orthopaedic applications. *Surf. Coat. Technol.* **2011**, *205*, 5260–5268. [[CrossRef](#)]
30. Chainani-wu, N. Safety and anti-inflammatory activity of curcumin: A component of tumeric (*Curcuma longa*). *J. Altern. Complement. Med.* **2003**, *9*, 161–168. [[CrossRef](#)]
31. Jurenka, J.S. Anti-inflammatory properties of curcumin, a major constituent of *Curcuma longa*: A review of preclinical and clinical research. *Altern. Med. Rev.* **2009**, *14*, 141–153. [[PubMed](#)]
32. Tyagi, P.; Singh, M.; Kumari, H.; Kumari, A.; Mukhopadhyay, K. Bactericidal activity of curcumin I is associated with damaging of bacterial membrane. *PLoS ONE* **2015**, *10*, e0121313. [[CrossRef](#)] [[PubMed](#)]
33. Nam, S.H.; Nam, H.Y.; Joo, J.R.; Baek, I.S.; Park, J. Curcumin-loaded PLGA nanoparticles coating onto metal stent by electrophoretic deposition techniques. *Bull. Korean Chem. Soc.* **2007**, *28*, 397–402. [[CrossRef](#)]
34. Zhang, J.; Wei, W.; Yang, L.; Pan, Y.; Wang, X.; Wang, T.; Tang, S.; Yao, Y.; Hong, H.; Wei, J. Stimulation of cell responses and bone ingrowth into macro-microporous implants of nano-bioglass/polyetheretherketone composite and enhanced antibacterial activity by release of hinokitiol. *Colloids Surf. B Biointerfaces* **2018**, *164*, 347–357. [[CrossRef](#)] [[PubMed](#)]
35. Miola, M.; Vernè, E.; Piredda, A.; Seuss, S.; Cabanas-Polo, S.; Boccaccini, A.R. Development and characterization of PEEK/B₂O₃-doped 45S5 bioactive glass composite coatings obtained by electrophoretic deposition. *Key Eng. Mater.* **2015**, *654*, 3–7. [[CrossRef](#)]
36. Seuss, S.; Heinloth, M.; Boccaccini, A.R. Development of bioactive composite coatings based on combination of PEEK, bioactive glass and Ag nanoparticles with antibacterial properties. *Surf. Coat. Technol.* **2015**, *301*, 100–105. [[CrossRef](#)]
37. Moskalewicz, T.; Zych, A.; ukaszczyk, A.; Cholewa-Kowalska, K.; Kruk, A.; Dubiel, B.; Radziszewska, A.; Berent, K.; Gajewska, M. Electrophoretic deposition, microstructure, and corrosion resistance of porous sol-gel glass/polyetheretherketone coatings on the Ti–13Nb–13Zr alloy. *Metall. Mater. Trans. A Phys. Metall. Mater. Sci.* **2017**, *48*, 2660–2673. [[CrossRef](#)]
38. Pishbin, F.; Mouriño, V.; Flor, S.; Kreppel, S.; Salih, V.; Ryan, M.P.; Boccaccini, A.R. Electrophoretic deposition of gentamicin-loaded bioactive glass/chitosan composite coatings for orthopaedic implants. *ACS Appl. Mater. Interfaces* **2014**, *6*, 8796–8806. [[CrossRef](#)]

39. Heise, S.; Höhlinger, M.; Hernández, Y.T.; Palacio, J.J.P.; Ortiz, J.A.R.; Wagener, V.; Virtanen, S.; Boccaccini, A.R. Electrophoretic deposition and characterization of chitosan/bioactive glass composite coatings on Mg alloy substrates. *Electrochim. Acta* **2017**, *232*, 456–464. [[CrossRef](#)]
40. Parchovianský, M.; Balko, J.; Švančárek, P.; Sedláček, J.; Dusza, J.; Lofaj, F.; Galusek, D. Mechanical properties and sliding wear behaviour of Al₂O₃-SiC nanocomposites with 3–20 vol.% SiC. *J. Eur. Ceram. Soc.* **2017**, *3*, 4297–4306. [[CrossRef](#)]
41. Balázsi, C.; Fogarassy, Z.; Tapasztó, O.; Kailer, A.; Schröder, C.; Parchoviansky, M.; Galusek, D.; Dusza, J.; Balázsi, K. Si₃N₄/graphene nanocomposites for tribological application in aqueous environments prepared by attritor milling and hot pressing. *J. Eur. Ceram. Soc.* **2017**, *37*, 3797–3804. [[CrossRef](#)]
42. Kokubo, T.; Takadama, H. How useful is SBF in predicting in vivo bone bioactivity? *Biomaterials* **2006**, *27*, 2907–2915. [[CrossRef](#)] [[PubMed](#)]
43. Godfrey, D. Friction oscillations with a pin-on-disc tribometer. *Tribol. Int.* **1995**, *28*, 119–126. [[CrossRef](#)]
44. Blau, P.J. The significance and use of the friction coefficient. *Tribol. Int.* **2001**, *34*, 585–591. [[CrossRef](#)]
45. Moskalewicz, T.; Zimowski, S.; Zych, A.; Łukaszczyk, A.; Reczyńska, K.; Pamuła, E. Electrophoretic deposition, microstructure and selected properties of composite alumina/polyetheretherketone coatings on the Ti-13Nb-13Zr alloy. *J. Electrochem. Soc.* **2018**, *165*, D116–D128. [[CrossRef](#)]
46. Atiq, M.; Rehman, U.; Bastan, F.E.; Nawaz, Q.; Boccaccini, A.R. Electrophoretic deposition of lawsone loaded nanoscale silicate glass/chitosan composite on PEEK/BG layers. *Electrochem. Soc. Trans.* **2018**, *82*, 45–50. [[CrossRef](#)]
47. Mehdipour, M.; Afshar, A. A study of the electrophoretic deposition of bioactive glass-chitosan composite coating. *Ceram. Int.* **2012**, *38*, 471–476. [[CrossRef](#)]
48. Shi, Y.Y.; Li, M.; Liu, Q.; Jia, Z.J.; Xu, X.C.; Cheng, Y.; Zheng, Y.F. Electrophoretic deposition of graphene oxide reinforced chitosan-hydroxyapatite nanocomposite coatings on Ti substrate. *J. Mater. Sci. Mater. Med.* **2016**, *27*, 48. [[CrossRef](#)]
49. Avcu, E.; Yasemin, Y.; Erdem, F.; Atiq, M.; Rehman, U.; Üstel, F.; Boccaccini, A.R. Tailoring the surface characteristics of electrophoretically deposited chitosan-based bioactive glass composite coatings on titanium implants via grit blasting. *Prog. Org. Coat.* **2018**, *123*, 362–373. [[CrossRef](#)]
50. Atiq, M.; Rehman, U.; Azeem, M.; Schubert, D.W.; Boccaccini, A.R. Electrophoretic deposition of chitosan/gelatin/bioactive glass composite coatings on 316L stainless steel: A design of experiment study. *Surf. Coat. Technol.* **2019**, *358*, 976–986. [[CrossRef](#)]
51. Avcu, E.; Bastan, F.E.; Abdullah, H.Z.; Rehman, M.A.U.; Avcu, Y.Y.; Boccaccini, A.R. Electrophoretic deposition of chitosan-based composite coatings for biomedical applications: A review. *Prog. Mater. Sci.* **2019**, *103*, 69–108. [[CrossRef](#)]
52. Batmanghelich, F.; Ghorbani, M. Effect of pH and carbon nanotube content on the corrosion behavior of electrophoretically deposited chitosan-hydroxyapatite-carbon nanotube composite coatings. *Ceram. Int.* **2013**, *39*, 5393–5402. [[CrossRef](#)]
53. Mahmoodi, S.; Sorkhi, L.; Farrokhi-Rad, M.; Shahrabi, T. Electrophoretic deposition of hydroxyapatite-chitosan nanocomposite coatings in different alcohols. *Surf. Coat. Technol.* **2013**, *216*, 106–114. [[CrossRef](#)]
54. Mouriño, V.; Boccaccini, A.R. Bone tissue engineering therapeutics: Controlled drug delivery in three-dimensional scaffolds. *J. R. Soc. Interface* **2010**, *7*, 209–227. [[CrossRef](#)]
55. Vallet-Regí, M.; Balas, F.; Arcos, D. Mesoporous materials for drug delivery. *Angew. Chem. Int. Ed.* **2007**, *46*, 7548–7558. [[CrossRef](#)]
56. Canal, C.; Pastorino, D.; Mestres, G.; Schuler, P.; Ginebra, M.P. Relevance of microstructure for the early antibiotic release of fresh and pre-set calcium phosphate cements. *Acta Biomater.* **2013**, *9*, 8403–8412. [[CrossRef](#)] [[PubMed](#)]
57. Hixson, A.W.; Crowell, J.H. Dependence of reaction velocity upon surface and agitation. *Ind. Eng. Chem.* **1931**, *23*, 1160–1168. [[CrossRef](#)]
58. Kopcha, M.; Lordi, N.G.; Tojo, K.J. Evaluation of release from selected thermosoftening vehicles. *J. Pharm. Pharmacol.* **1991**, *43*, 382–387. [[CrossRef](#)]
59. Teow, S.; Liew, K.; Ali, S.A.; Khoo, A.S.; Peh, S. Antibacterial action of curcumin against staphylococcus aureus: A brief review. *J. Trop. Med.* **2016**, *2016*, 2853045. [[CrossRef](#)]

60. Seuss, S.; Lehmann, M.; Boccaccini, A.R. Alternating current electrophoretic deposition of antibacterial bioactive Glass-Chitosan composite coatings. *Int. J. Mol. Sci.* **2014**, *15*, 12231–12242. [[CrossRef](#)]
61. Hoppe, A.; Meszaros, R.; Stähli, C.; Romeis, S.; Schmidt, J.; Peukert, W.; Marelli, B.; Nazhat, S.N.; Wondraczek, L.; Lao, J.; et al. In vitro reactivity of Cu doped 45S5 Bioglass® derived scaffolds for bone tissue engineering. *J. Mater. Chem. B* **2013**, *1*, 5659. [[CrossRef](#)]
62. Hench, L.L.; Jones, J.R. Bioactive glasses: Frontiers and challenges. *Front. Bioeng. Biotechnol.* **2015**, *3*, 1–12. [[CrossRef](#)] [[PubMed](#)]



© 2019 by the authors. Licensee MDPI, Basel, Switzerland. This article is an open access article distributed under the terms and conditions of the Creative Commons Attribution (CC BY) license (<http://creativecommons.org/licenses/by/4.0/>).